Supporting Information for

Template-free synthesis of wafer-sized polyaniline nanoscale film with high electrical conductivity for trace ammonia gas sensing

Chonghui Zhu[#[a,c]], Xin Dong[#[a,b]], Chuanyu Guo[[a]], Lihua Huo[[a]], Shan Gao[[a]], Zhikun Zheng[*[b]], Xiaoli Cheng[*[a]], Yingming Xu[*[a]]

[a] Key Laboratory of Functional Inorganic Material Chemistry, Ministry of Education, School of Chemistry and Materials Science Heilongjiang University, Harbin, 150080, P.R. China.

[b] Key Laboratory for Polymeric Composite and Functional Materials of Ministry of Education, School of Chemistry and State Key Laboratory of Optoelectronic Materials and Technologies, Sun Yat-sen University, Guangzhou, P. R. China.

[c] State Key Laboratory of Integrated Optoelectronics, College of Electronic Science and Engineering, Jilin University, Changchun 130012, P.R. China.

E-mail: zhengzhikun@mail.sysu.edu.cn

E-mail: chengxiaioli@hlju.edu.cn

E-mail: xuyingming@hlju.edu.cn.

Table of contents

Characterization of PANI films.

The structure of the PANI nanoscale thin film was tested by a grazing incidence wide angle X-ray scattering (GIWAXS) meter model Xeuss 2.0 manufactured by Xenocs, France. The incident source was a liquid metal target source manufactured by Excillum, model number MetalJet D2, with a wavelength of 0.134144 nm and a lens-to-sample distance of 218.308 mm. The morphology and thickness of the PANI nanoscale thin films were investigated by a scanning electron microscope model S-4800 manufactured by Hitachi, Japan, and an atomic force microscope model MultiMode8 manufactured by Bruker Corporation. The microstructures of the films were studied by a transmission electron microscope model number JEOL-JEM-2010, and the high-resolution transmission electron microscope and the selected area electron diffraction pattern of the films were further tested. This operating voltage of the instrument was 200 kV. Electrochemical performance is measured by CHI600E series electrochemical analyzer manufactured by Shanghai Chenhua Instrument Company.

Conductivity measurement.

The content of the oxidant has a certain effect on the conductivity of the PANI nanoscale thin film, for which we conducted research. The APS content in the reaction system is changed to 10.8, 5.4, 3.2, and 2.1 $mmol \cdot L^{-1}$. When the APS content is 2.1 $mmol \cdot L^{-1}$, the PANI nanoscale thin film is difficult to form. Therefore, combined with the thickness of the film (Figure S6) and I-V curves (Figure S8a), the conductivity of the other three PANI films are calculated, and their value are 8.54×10^{-4}, 5.19 and 109.05 $S \cdot cm^{-1}$, respectively. The results show that when the oxidant content increases, the crystallinity of the film becomes worse, which leads to a decrease in the electrical conductivity of the film. This phenomenon is also seen from the GIWAXS characterization (Figure S9). When the APS content is 3.2 $mmol \cdot L^{-1}$, the reaction temperatures are changed by $10^{o}C$ to $1^{o}C$, the reaction times are 2 to 10 days, and the effect of different reaction conditions to the conductivity is studied. According to the I-V curves (Figure S8b-d) and AFM spectrums (Figure S2) of the synthesized PANI nanoscale thin

films at different temperatures and different times, the conductivity was calculated, and the results are shown in Table S2. The higher reaction temperature increases the thickness of the film and reduces its conductivity. Too short or too long a reaction time also affects the thickness and crystallinity of the film, and also leads to a decrease in its electrical conductivity. Based on the above results, we can determine that the reaction temperature is 1^{o}C, and the reaction time is 7 days, the synthetic PANI nanoscale thin film has better conductivity.

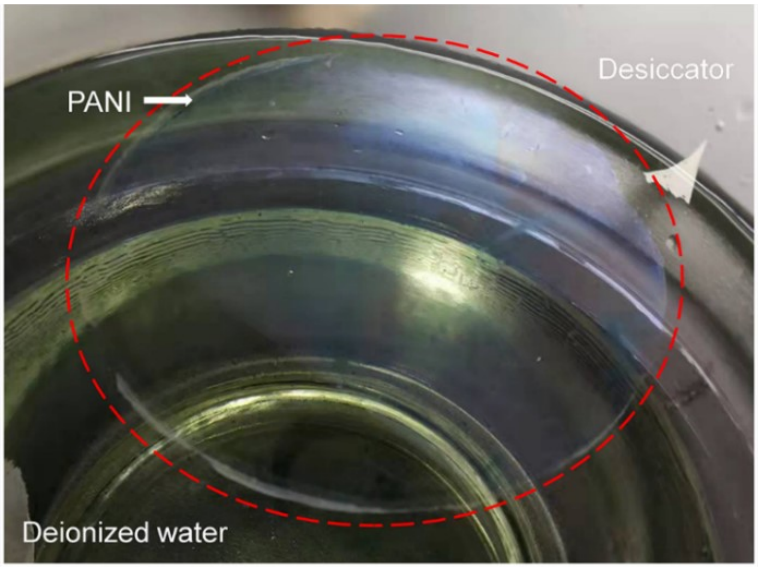

Figure S1. Photograph of the PANI nanoscale thin film on the water interface.

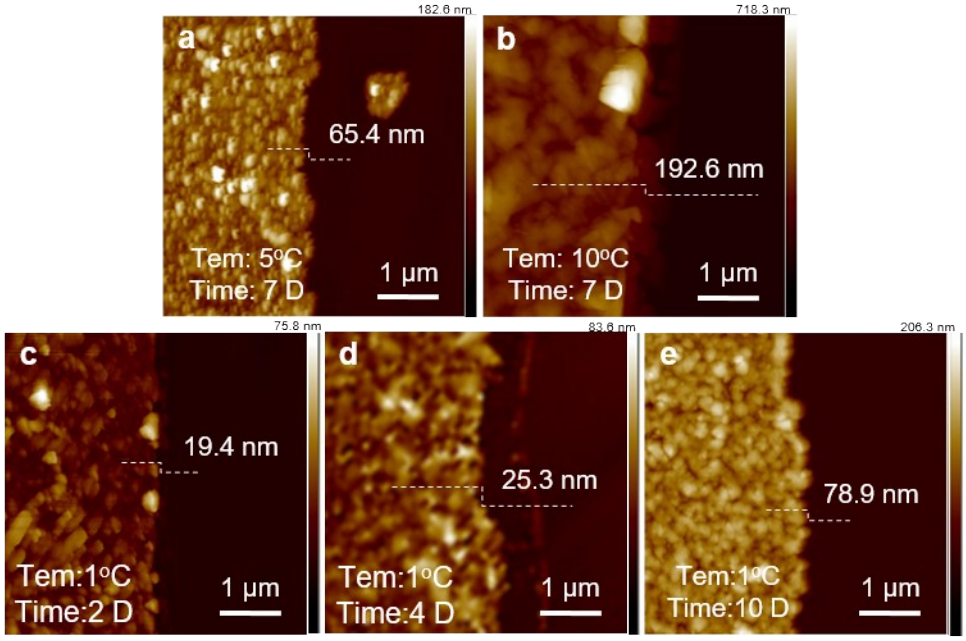

Figure S2. AFM images and thickness of the PANI nanoscale thin films at different reaction temperatures and different reaction times.

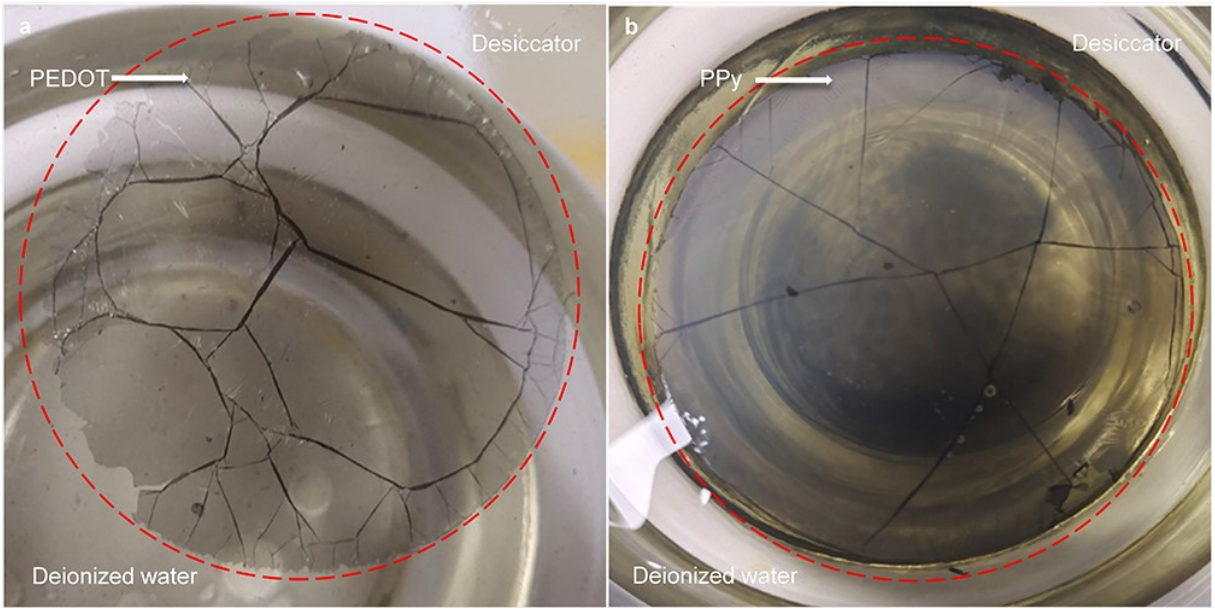

Figure S3. Photograph of PEDOT and PPy films on the water interface.

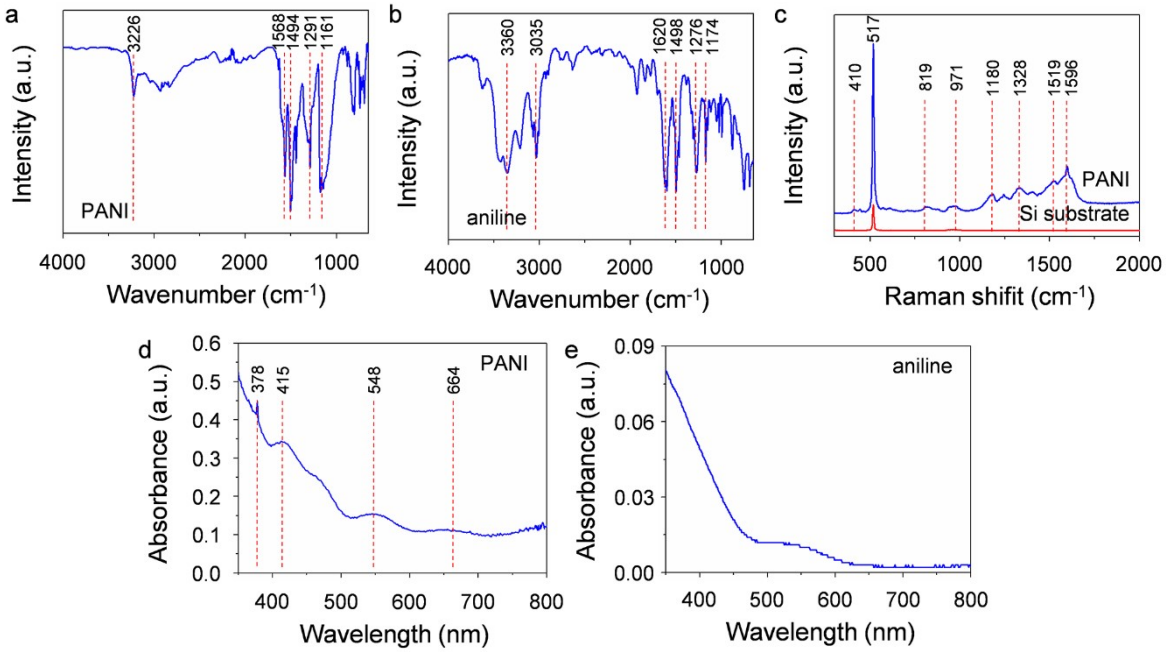

Figure S4. FTIR (a), Raman (b) and UV-vis (c) spectrums of the PANI nanoscale thin film. FTIR (d) and UV-vis (e) spectrums of aniline.

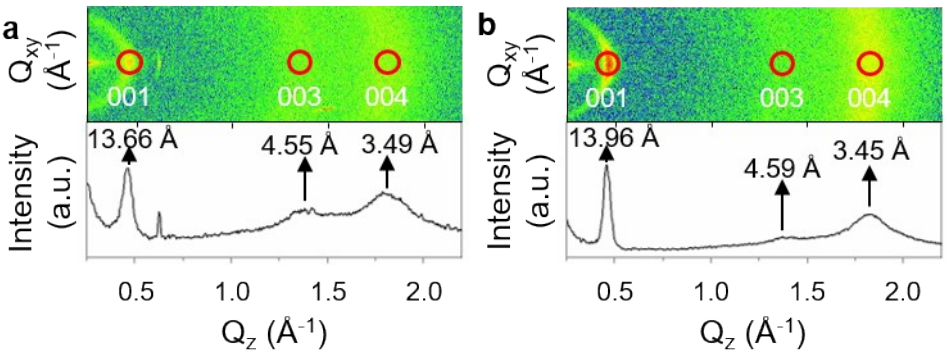

Figure S5. Grazing-incidence wide-angle X-ray scattering patterns and the projections of the transition from PANI thin films at (a) 10.8 and (b) 5.4 mmol APS on SiO_2/Si wafer.

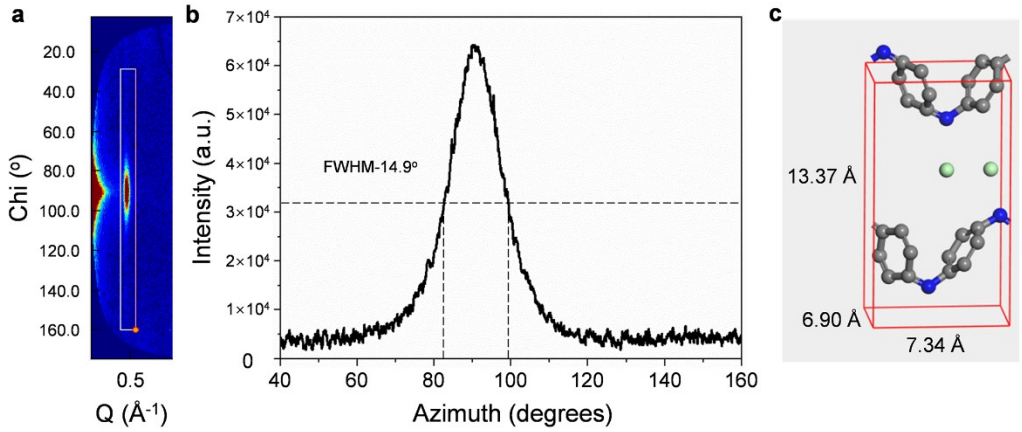

Figure S6. Degree of orientation of PANI film (a), 2D Azimuthal-angle-to-Q diagram with selected area 0.4 Å^{-1} <*Q*< *0.55* Å^{-1} and 40° < Chi <160°. (b) Azimuthal intensity distribution of the selected area in (a), corresponding to (001) Bragg peak of PANI film. (c) Structure of PANI film.

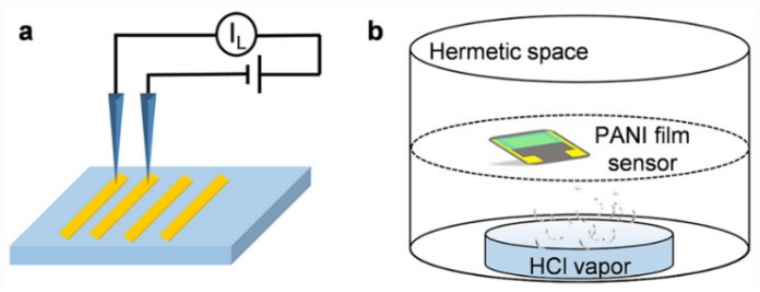

Figure S7. Illustrations of electrical measurements (a) and preparation of HCl doped the PANI nanoscale thin film (b).

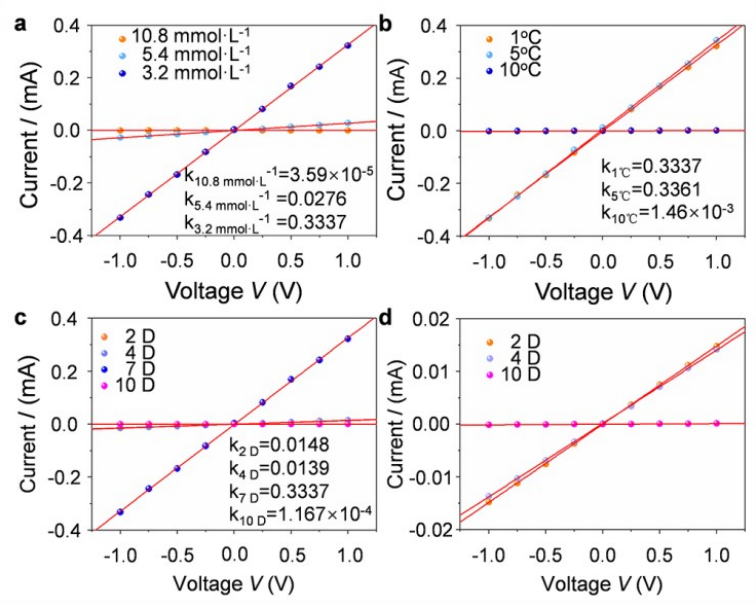

Figure S8. I-V curves of the PANI nanoscale thin films at different (a) APS contents, (b) different temperatures, and (c, d) different reaction times.

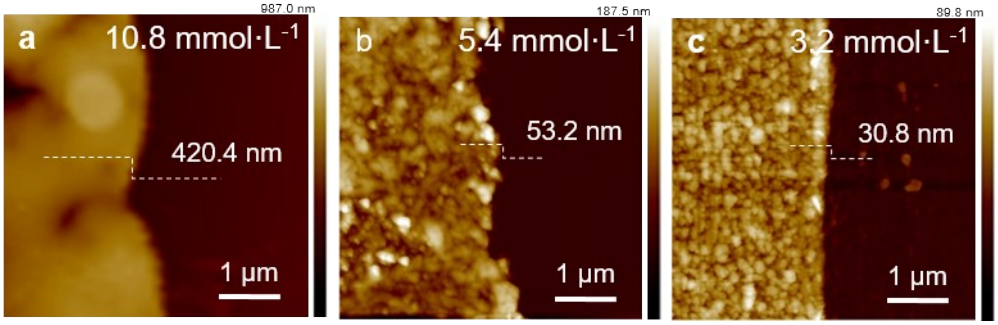

Figure S9. AFM images and thickness of the PANI nanoscale thin films at different APS content.

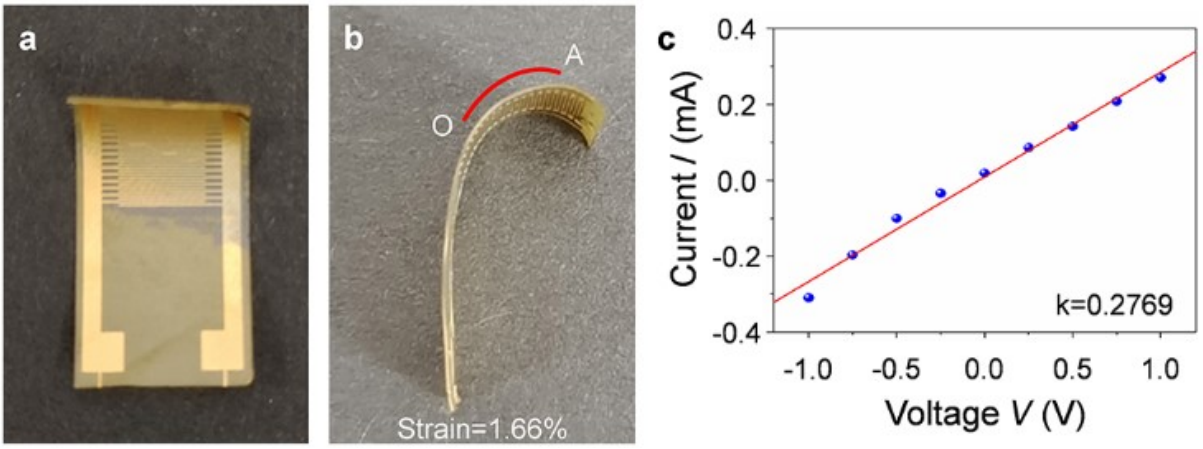

Figure S10. Strain value of the film after bending. The curvature radius (R_{OA}) and strain value of the PANI nanoscale thin film after bending is 3.0 mm and 1.66%, respectively (a, b). I-V curve of the PANI nanoscale thin film after 100 bending (c).

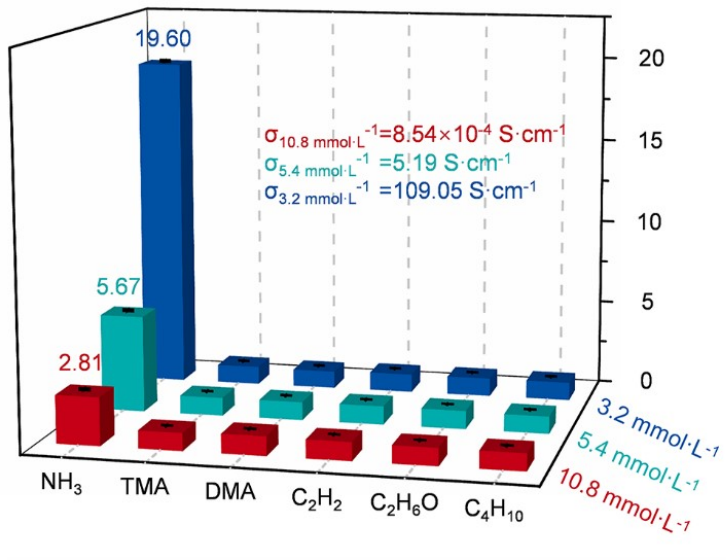

Figure S11. The selectivity of the PANI nanoscale thin films with different conductivity to 100 ppm six gases.

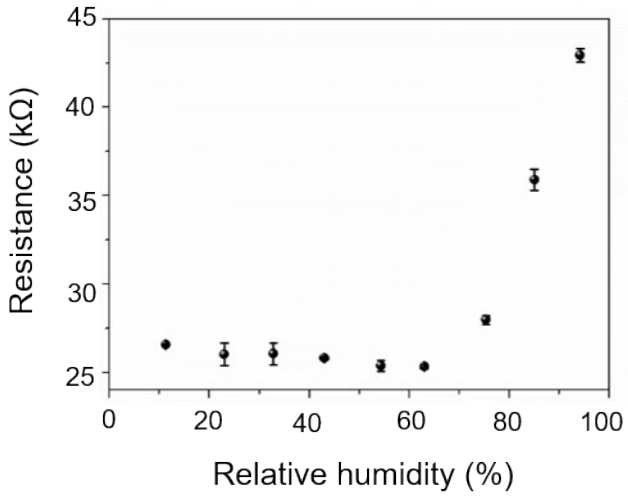

Figure S12. The resistance of PANI film sensor at different relative humidity

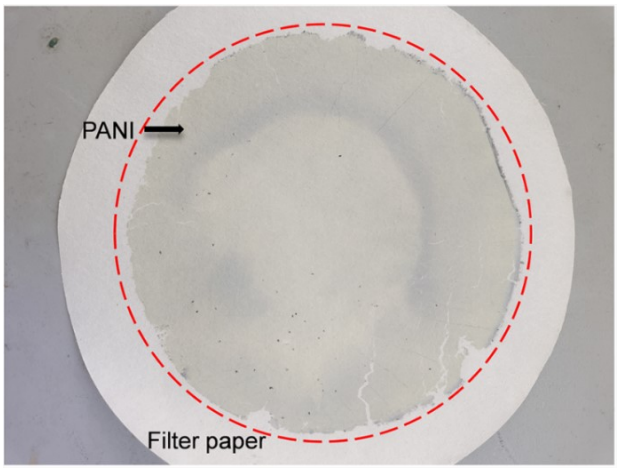

Figure S13. Photograph of the PANI nanoscale thin film on a filter paper.

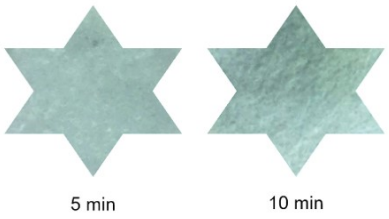

Figure S14 The paper-based sensor in 1.5 ppm NH_3

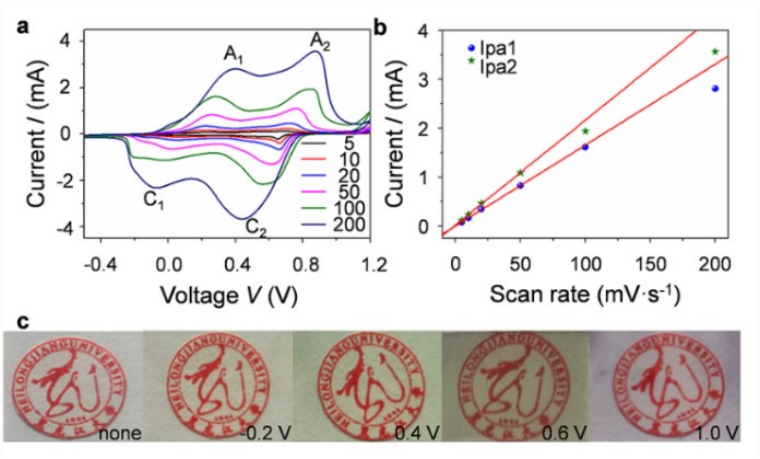

Figure S15. CV curves of the PANI nanoscale thin films with different sweep speed in 1 mol·L^{-1} HCl (a). The relationship between oxidation peak current density and scan rate (b). Color changes of the PANI nanoscale thin films at different voltages (c).

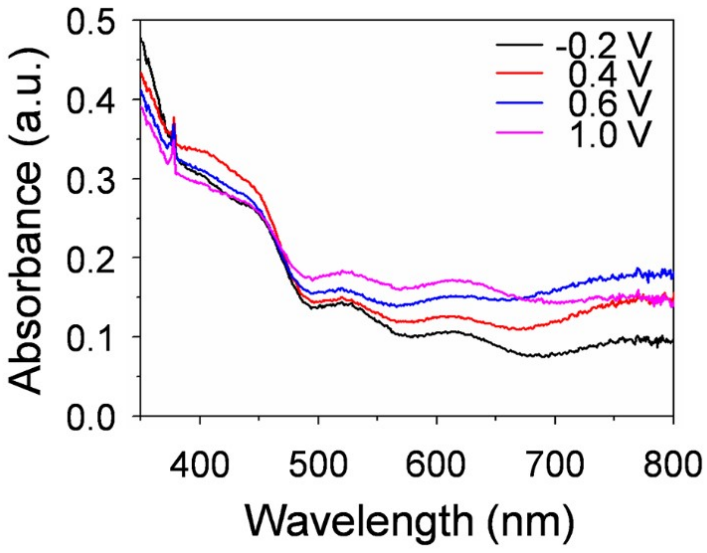

Figure S16. UV-vis spectra of the PANI nanoscale thin films with different voltage.

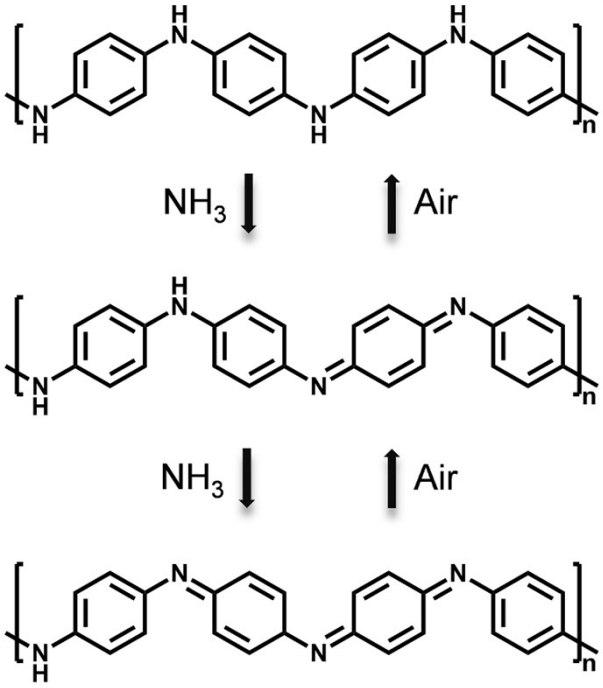

Figure S17. PANI film sensor gas sensing mechanism.

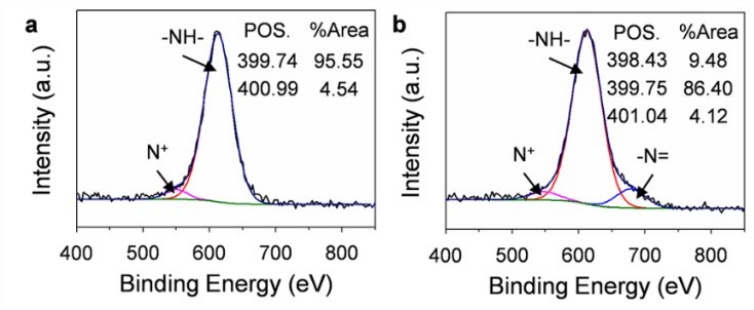

Figure S18. XPS spectra of N 1s before (a) and after (b) adsorption of NH_3.

Table S1. Assignments of the FTIR bands for PANI and aniline.

Wavenumber (cm^{-1})		Assignment
PANI	aniline	
	3433	N-H stretches (primary amines)
	3356	N-H stretches (primary amines)
3226		N-H vibration
	3035	Shoulder band
	1620	N-H stretches (primary amines)
1568		C=C stretch vibration of the quinoid ring
1490	1498	C=C stretch vibration of thebenzenoid ring
1291	1276	C-N stertching
1161	1174	plane bending of C-H

Table S2. Material conductivity and film thickness on flexible interdigital electrodes in polyimide (PI) substrates

	Oxidizer content ($mmol \cdot L^{-1}$)			**Different temperature (°C)**			**Different time (days)**			
Materials	10.8	5.4	3.2	10	5	1	2	4	7	10
Conductivity ($S \cdot cm^{-1}$)	8.54×10^{-4}	5.19	109.05	0.075	58.99	109.05	7.63	5.49	109.05	0.0148
Thickness (nm)	420.4	53.2	30.6	192.6	65.4	30.6	19.4	25.3	30.6	78.9

Table S3. The comparison of response to NH_3 between the PANI film sensor in this work and the PANI-based film sensors in the articles

Sensing material	Response/NH_3 concentration	Response time	Recovery time	Detection limit	Detection range	Substrate	Ref.
PANI film	19.46/100 ppm	100 s	26 s	2 ppb	2 ppb-100 ppm	flexible	This work
PANI	1.07/120 ppb	11.5 min	-	30 ppb	30-120 ppb	stiffness	20
PANI-CNT	30/100 ppm	~250 s	200 s	1 ppm	1-100 ppm	flexible	15
PVDF-PANI	1.38/80 ppm	2.5 min	~15 min	100 ppb	0.01-10 ppm	stiffness	1
PANI/rGO	67/100 ppm	36 s	18 s	100 ppb	0.01-100 ppm	flexible	2
GO-PANIHs	31.8/100 ppm	102 s	186 s	50 ppb	50 ppb-100 ppm	flexible	3
PANI-MWCNTs	3.55/100 ppm	120 s	137 s	0.01 ppm	0.01-100 ppm	flexible	4
MWCNTs-PANI	2.092/100 ppm	9 s	30 s	0.2 ppm	0.2-100 ppm	flexible	5
SiO_2/PANI	10/100 ppm	500 s	500 s	400 ppb	0.04-300 ppm	flexible	6
BC/PANI-DBSA	6.1/100 ppm	10.2 s	8.6 s	0.2 ppm	0.2-150 ppm	flexible	7
PANI/Ge	10.98/50 ppm	72 s	111 s	-	20, 50 ppm	flexible	8
PANI-WO_3	2.21/100 ppm	30 s	170 s	1 ppm	1-100 ppm	flexible	9
PANI/$SrGe_4O_9$	3.08/10 ppm	108 s	320 s	0.25 ppb	0.2-10 ppm	flexible	17
PANI/Nb_2CTx	1.75/10 ppm	-	-	20 ppb	0.1-50 ppm	flexible	20
Mn_3O_4/Fe_2O_3	65/25 ppm	1 min	16 min	2 ppm	5-30 ppm	stiffness	10
Sn/SnO_2	142.2/300 ppm	148 s	136 s	5 ppm	5-1000 ppm	stiffness	11
ZnO/CuPc	15.8/100 ppm	20 s	10 s	0.8 ppm	0.8-100 ppm	stiffness	12
Mn-TiO_2	2188/20 ppm	21 s	24 s	5 ppm	5-40 ppm	stiffness	13
rGO-SiO_2	1.12/50 ppm	250 s	~250 s	5 ppm	5-100 ppm	stiffness	14
C-ny graphene	1.28/50 ppm	13 min	-	50 ppm	50-4000 ppm	stiffness	15
Au/PPy	26.5/100 ppm	26.5 s	7 s	1 ppm	1-100 ppm	flexible	16
PPy	1.11/100 ppm	~10 min	~15 min	0.4 ppm	0.2-100 ppm	stiffness	17

Reference

1. J.L. Wojkiewicz, V.N. Bliznyuk, S. Carquigny, N. Elkamchi, N. Redon, T. Lasri, A.A. Pud, S. Reynaud, *Sensors Actuators, B Chem.* **2011**, *160*, 1394–1403.
2. Y. Guo, T. Wang, F. Chen, X. Sun, X. Li, Z. Yu, P. Wan, X. Chen, *Nanoscale* **2016**, *8*, 12073–12080
3. S. Li, T. Wang, Z. Yang, J. He, J. Wang, L. Zhao, H. Lu, T. Tian, F. Liu, P. Sun, X. Yan, G. Lu, *Sensors Actuators, B Chem.* **2018**, *273*, 726–734.
4. S. Wang, G. Xie, H. Tai, Y. Su, B. Yang, Q. Zhang, X. Du, Y. Jiang, *Nano Energy* **2018**, *51*, 231–240.
5. D. Maity, R.T.R. Kumar, *ACS Sensors* **2018**, *3*, 1822–1830.
6. Q. Nie, Z. Pang, D. Li, H. Zhou, F. Huang, Y. Cai, Q. Wei, *Colloids Surfaces A Physicochem. Eng. Asp.* **2018**, *537*, 532–539.
7. L. Yang, S. Wu, F. Wei, Y. Hu, X. Xu, L. Zhang, D. Sun, *Sensors Actuators, B Chem.* **2020**, *323*, 128689.
8. L. Li, G. Li, W. Zhang, C. She, J. Lin, S. Liu, F. Yue, C. Jing, Y. Cheng, J. Chu, *Mater. Lett.* **2020**, *278*, 128438.
9. S.B. Kulkarni, Y.H. Navale, S.T. Navale, F.J. Stadler, N.S. Ramgir, V.B. Patil, *Sensors Actuators, B Chem.* **2019**, *288*, 279–288.
10. L. Bigiani, D. Zappa, C. Maccato, A. Gasparotto, C. Sada, E. Comini, D. Barreca, *Adv. Mater. Interfaces* **2019**, 6, 34–36.
11. A.M. Al-Enizi, M. Naushad, A.H. Al-Muhtaseb, S.M. Alshehri, Z.A. Alothman, T. Ahamad, *Chem. Eng. J.* **2018**, *345*, 58-66.
12. J. Huang, D. Jiang, J. Zhou, J. Ye, Y. Sun, X. Li, Y. Geng, J. Wang, Y. Du, Z. Qian, *Sensors Actuators, B Chem.* **2021**, *327*, 128911.
13. P.T. Zamaswazi, S. Katekani, R.C. Franscious, M.N. Odireleng, H.M. Gugu, E.M. David, *J. Colloid Interface Sci.* **2017**, *504*, 371–386.
14. D. Huang, Z. Yang, X.L. Li, L.L. Zhang, J. Hu, Y. Su, N.T. Hu, G.L. Yin, D. He, Y. Zhang, *Nanoscale* **2017**, *9*, 109–118.

15. M.K. Rabchinskii, A.S. Varezhnikov, V.V. Sysoev, M.A. Solomatin, S.A. Ryzhkov, M.V. Baidakova, D.Y. Stolyarova, V.V. Shnitov, S.S. Pavlov, D.A. Kirilenko, A.V. Shvidchenko, E.Y. Lobanova, M.V. Gudkov, D.A. Smirnov, V.A. Kislenko, S.V. Pavlov, S.A. Kislenko, N.S. Struchkov, I.I. Bobrinetskiy, A.V. Emelianov, P. Liang, Z. Liu, P.N. Brunkov, *Carbon* **2021**, *172*, 236–247.

16. Z.Y. Li, J.Y. Chen, L. Chen, M.L. Guo, Y.P. Wu, Y. Wei, J.F. Wang, X.G. Wang, *ACS Appl. Mater. Interfaces* **2020**, *12*, 55056−55063.

17. D. Kim, B. Yoo, *Sensors Actuators, B Chem.* **2011**, *160*, 1168–1173.